

# Pattern formation by kicked solitons in the two-dimensional Ginzburg-Landau medium with a transverse grating

Valentin Besse<sup>1</sup>, Hervé Leblond<sup>1</sup>, Dumitru Mihalache<sup>1,2,3</sup> and Boris A. Malomed<sup>4</sup>

<sup>1</sup> *LUNAM Université, Université d'Angers, Laboratoire de Photonique d'Angers, EA 4464, 2 Bd Lavoisier, 49000 Angers, France*

<sup>2</sup> *Horia Hulubei National Institute for Physics and Nuclear Engineering, 30 Reactorului, Magurele-Bucharest, 077125, Romania*

<sup>3</sup> *Academy of Romanian Scientists, 54 Splaiul Independentei, 050094 Bucharest, Romania*

<sup>4</sup> *Department of Physical Electronics, Faculty of Engineering, Tel Aviv University, Tel Aviv 69978, Israel*

We consider the kick-induced mobility of two-dimensional (2D) fundamental dissipative solitons in models of lasing media based on the 2D complex Ginzburg-Landau (CGL) equation including a spatially periodic potential (transverse grating). The depinning threshold is identified by means of systematic simulations, and described by means of an analytical approximation, depending on the orientation of the kick. Various pattern-formation scenarios are found above the threshold. Most typically, the soliton, hopping between potential cells, leaves arrayed patterns of different sizes in its wake. In the laser cavity, this effect may be used as a mechanism for selective pattern formation controlled by the tilt of the seed beam. Freely moving solitons feature two distinct values of the established velocity. Elastic and inelastic collisions between free solitons and pinned arrayed patterns are studied too.

PACS numbers: 42.65.Tg, 42.65.Sf, 47.20.Ky

## I. INTRODUCTION

A well-known fact is that the formation of stable dissipative solitons—most typically, in lasing media [1] and plasmonic cavities [2]—relies upon the simultaneous balance of competing conservative and dissipative effects in the system, i.e., respectively, the diffraction and self-focusing nonlinearity, and linear and nonlinear loss and gain [3]. The generic model describing media where stable dissipative solitons emerge via this mechanism is based on the complex Ginzburg-Landau (CGL) equations with the cubic-quintic (CQ) combination of gain and loss terms, which act on top of the linear loss [1]. In addition to modeling the laser-physics and plasmonic settings, the CGL equations, including their CQ variety, serve as relevant models in many other areas, well-known examples being Bose-Einstein condensates in open systems (such as condensates of quasi-particles in solid-state media) [4], reaction-diffusion systems, and superconductivity. Thus, the CGL equations constitute a class of universal models for the description of nonlinear waves and pattern formation in dissipative media [5].

The CGL equation with the CQ nonlinearity was originally postulated by Petviashvili and Sergeev [6] as a model admitting stable localized two-dimensional (2D) patterns. Subsequently, a great deal of 1D and 2D localized solutions, i.e., dissipative solitons, have been studied in detail in the framework of systems of this type [7]-[9].

A 2D model of laser cavities with an internal transverse grating, based on the CQ-CGL equation with a spatially periodic (lattice) potential, which represents the grating, was introduced in Ref. [10]. Note that the available laser-writing technology makes it possible to fabricate permanent gratings in bulk media [11]. In addition, in photorefractive crystals virtual photonic lattices may be induced by pairs of pump laser beams with the ordinary polarization, which illuminate the sample in the directions of  $x$  and  $y$ , while the probe beam with the extraordinary polarization is launched along axis  $z$  [12]. In fact, the laser cavity equipped with the grating may be considered as a photonic crystal built in the active medium.

A notable fact reported in Ref. [10] is that localized vortices, built as sets of four peaks pinned to the periodic potential, may be stable without the presence of the unphysical diffusion term in the CGL laser model, which is necessary for the stabilization of dissipative vortex solitons in uniform media, see, e.g., Ref. [8]. In subsequent works, stable fundamental and vortical solitons in 2D [13] and 3D [14] CGL models with trapping potentials were studied in detail. Spatiotemporal dissipative solitons in the CQ-CGL model of 3D laser cavities including the transverse grating were investigated too [14]. Both fundamental and vortical solitons were found in a numerical form as attractors in the latter model, and their stability against strong random perturbations was tested by direct simulations.

While the stability of various 2D localized patterns has been studied thoroughly in the framework of the CQ-CGL equations with the transverse lattice potential used as the stabilizing factor, a challenging problem is mobility of such 2D dissipative solitons under the action of a kick applied across the underlying lattice. In terms of the laser cavities, the mobility is an issue of obvious physical relevance, as it implies a possibility to generate oblique beams. Furthermore, it is shown in this paper that hopping motion of the kicked soliton through cells of the periodic potential can be used for controlled creation of various patterns filling these cells (or a part of them). An obvious obstacle to

the mobility in this setting is the Peierls-Nabarro (PN) barrier induced by the underlying potential.

The objective of this work is to study the mobility of the 2D fundamental solitons, and scenarios of the pattern formation by kicked solitons, in the framework of the CQ-CGL models with the lattice potential. The model is formulated in Section II, which also presents an analytical approximation, that makes it possible to predict, with a reasonable accuracy, the minimum (threshold) strength of the kick necessary for depinning of the quiescent soliton trapped by the lattice. The main numerical results for the mobility of the kicked soliton, and various scenarios of the pattern creation in the wake of the soliton hopping between cells of the potential lattice are reported in Section III. In addition to that, Section IV deals with collisions between the freely moving soliton and a standing structure created and left by it, in the case of periodic boundary conditions (which correspond to a laser cavity in the form of a cylindrical surface). The paper is concluded by Section V.

## II. THE MODEL AND ANALYTICAL APPROXIMATIONS

### A. The Ginzburg-Landau equation

Following Refs. [10] and [13], the scaled CQ-CGL equation for the evolution of the amplitude of the electromagnetic field,  $u(X, Y, Z)$ , in two dimensions with transverse coordinates  $\mathbf{R} = (X, Y)$ , along the propagation direction,  $Z$ , is written as

$$\frac{\partial u}{\partial Z} = \left[ -\delta + iV(X, Y) + \frac{i}{2}\nabla_{\perp}^2 + (i + \epsilon)|u|^2 - (i\nu + \mu)|u|^4 \right] u, \quad (1)$$

where  $\nabla_{\perp}^2 = \partial^2/\partial X^2 + \partial^2/\partial Y^2$  is the transverse Laplacian, which represents the paraxial diffraction, real coefficients  $\delta$ ,  $\epsilon$ , and  $\mu$  account for the linear loss, cubic gain, and quintic loss, respectively, and  $\nu$  is the quintic self-defocusing coefficient, which accounts for the saturation of the Kerr nonlinearity, if  $\nu > 0$ . The transverse grating is represented by the periodic potential,

$$V(X, Y) = -V_0 [\cos(2X) + \cos(2Y)], \quad (2)$$

of depth  $2V_0$ , with the period scaled to be  $\pi$ . Dissipative solitons produced by Eq. (1) are characterized by the total power,

$$P = \int \int |u(X, Y, Z)|^2 dX dY. \quad (3)$$

In the simulations, Eq. (1) was solved by means of the standard fourth-order Runge-Kutta scheme in the  $Z$ -direction, and five-point finite-difference approximation for the transverse Laplacian. As specified below, we used periodic boundary conditions. The integration domain correspond to a  $(X, Y)$  matrix of  $256 \times 256$  grid points from  $X_{min} = -22$  to  $X_{max} = 22$  (same distance for  $Y$  dimension). Generic results for the mobility of fundamental dissipative solitons can be adequately represented by fixing the following set of parameters:

$$\delta = 0.4, \epsilon = 1.85, \mu = 1, \nu = 0.1, V_0 = 1, \quad (4)$$

for which the quiescent fundamental soliton is stable.

The kick was applied, as usual, by multiplying the initial steady state,  $u_0$ , by  $\exp(i\mathbf{k}_0\mathbf{R})$ , with the vectorial strength of the kick defined as

$$\mathbf{k}_0 = (k_0 \cos \theta, k_0 \sin \theta), \quad (5)$$

where it is sufficient to confine  $\theta$  to interval  $0 \leq \theta \leq \pi/4$ . In terms of the laser cavity, a small angle  $\varphi$  between the carrier wave vector  $\mathbf{K}_0$  of the beam and the  $Z$ -axis gives rise to the transverse component,  $k_0 = K_0 \sin \varphi$ , which corresponds to the kick. Below, we study the effects induced by the kick by varying its magnitude  $k_0$  and orientation angle  $\varphi$ . The first characteristic of kink-induced effects is the threshold value,  $(k_0)_{thr}$ , such that the soliton remains pinned at  $k_0 < (k_0)_{thr}$  and escapes at  $k_0 > (k_0)_{thr}$ .

## B. Analytical estimates

To develop an analytical approximation for dissipative solitons in the present model, one can, in the zero-order approximation, drop the loss and gain terms, as well as the lattice potential, in Eq. (1). The corresponding 2D nonlinear Schrödinger equation gives rise to the commonly known family of Townes soliton, which share a single value of the total power,  $P_T \approx 5.85$  [15]. The family may be effectively approximated by the isotropic Gaussian ansatz with arbitrary amplitude  $A$ ,

$$u\left(Z, R \equiv \sqrt{X^2 + Y^2}\right) = A \exp\left(ibZ - \frac{\pi A^2}{2P_T} R^2\right), \quad (6)$$

and propagation constant  $b = A^2/4$  [16]. Taking into regard the loss and gain terms as perturbations, one can predict the equilibrium value of the amplitude from the power-balance equation,

$$\delta P + \mu \int \int |u(X, Y)|^6 dX dY = \epsilon \int \int |u(X, Y)|^4 dX dY. \quad (7)$$

The substitution of approximation (6) into Eq. (7) leads to a quadratic equation for  $A^2$ , with roots

$$A^2 = \frac{3\epsilon \pm \sqrt{3(3\epsilon^2 - 16\delta\mu)}}{4\mu}, \quad (8)$$

the larger one corresponding to a stable dissipative soliton (cf. a similar analysis for the CQ-CGL model in 1D [17]).

Proceeding to the kicked soliton, the above-mentioned threshold magnitude of the kick for the depinning,  $(k_0)_{\text{thr}}$ , can be estimated from the comparison of the PN potential barrier,  $U_{\text{PN}}$ , and the kinetic energy of the kicked soliton,  $E_{\text{kin}}$ . The Galilean invariance of Eq. (1) [18] (in the absence of the lattice potential) implies that kick (5) gives rise to “velocity”  $\mathbf{k}_0$ , so that the solution will become a function of  $\mathbf{R} - \mathbf{k}_0 Z \equiv \mathbf{R} - \Upsilon$ , instead of  $\mathbf{R}$ , the corresponding kinetic energy being

$$E_{\text{kin}} = (1/2) P k_0^2 \quad (9)$$

( $P$  plays the role of the effective mass of the soliton). Further, assuming that the kicked soliton moves in the direction of  $\theta$  [see Eq. (5)], the effective energy of the interaction of the soliton, taken as per approximation (6), with lattice potential (2), treated as a perturbation, is

$$\begin{aligned} E_{\text{pot}}(\Upsilon) &= -V_0 \int \int [\cos(2X) + \cos(2Y)] |u(X - \Upsilon \cos \theta, Y - \Upsilon \sin \theta)|^2 dX dY \\ &= -V_0 P \exp\left(-\frac{P_T}{\pi A^2}\right) [\cos(2\Upsilon \cos \theta) + \cos(2\Upsilon \sin \theta)], \end{aligned} \quad (10)$$

where  $\Upsilon$  is the shift of the soliton from  $X = Y = 0$  in the direction of  $\theta$ . As follows from this expression, the PN barrier, i.e., the difference between the largest and smallest values of the potential energy, is estimated as

$$E_{\text{PN}} = V_0 P \exp\left(-\frac{P_T}{\pi A^2}\right) \Delta(\theta), \quad (11)$$

where  $\Delta(\theta)$  is the difference between the maximum and minimum of function  $\cos(2\Upsilon \cos \theta) + \cos(2\Upsilon \sin \theta)$ . Obviously,  $\Delta(0) = 2$  and  $\Delta(\pi/4) = 4$ . For intermediate values of  $\theta$ , it may be approximated by the difference of the values of the function between points  $\Upsilon = 0$  and  $\Upsilon = \pi/(2 \cos \theta)$ , i.e.,

$$\Delta(\theta) \approx 3 - \cos(\pi \tan \theta). \quad (12)$$

Finally, the threshold value of the kick is determined by the depinning condition,  $E_{\text{kin}} = E_{\text{PN}}$ , i.e.,

$$(k_0)_{\text{thr}} = \sqrt{2V_0 [3 - \cos(\pi \tan \theta)]} \exp\left(-\frac{P_T}{2\pi A^2}\right). \quad (13)$$

## III. NUMERICAL RESULTS: THE MOBILITY AND PATTERN FORMATION

The stable fundamental soliton constructed in the model based on Eqs. (1) and (2) at parameter values (4) is shown in Fig. 1. For parameters (4), analytical prediction (8) yields the amplitude of the stable soliton  $A \approx 1.496$ , which is quite close to the amplitude of the numerically found solution in Fig. 1.

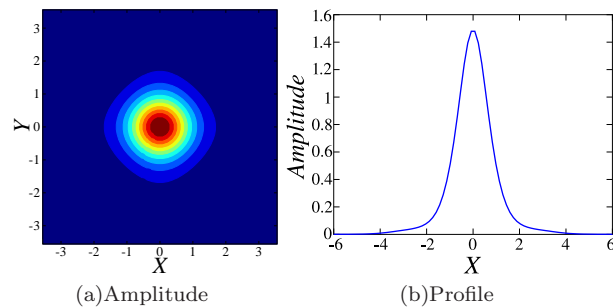


FIG. 1: (Color online) The stable fundamental soliton: (a) the contour plot of the local amplitude,  $|u(X, Y)|$ ; (b) the cross-section profile of  $|u(X)|$  at  $Y = 0$ .

### A. The formation of arrayed soliton patterns

First we consider the solitons kicked with  $\theta = 0$ , i.e., along bonds of the lattice, see Eq. (5). Below the threshold value of the kick's strength, whose numerically found value is

$$(k_0)_{\text{thr}}(\theta = 0) \approx 1.6865, \quad (14)$$

the kicked soliton exhibits damped oscillations, remaining pinned around a local minimum of the lattice potential, as shown in Fig. 2. Originally (at  $0 < z < 8$  in Fig. 2), the total power (3) increases, and then it drops to the initial value,  $P \approx 3.2$ . As a result of the kick, a portion of the wave field passes the potential barrier and penetrates into the adjacent lattice cell, but, at  $k_0 < (k_0)_{\text{thr}}$ , the power carried by the penetrating field is not sufficient to create a new soliton, and is eventually absorbed by the medium.

On the other hand, analytical prediction (13) yields  $(k_0)_{\text{thr}}(\theta = 0) \approx 1.32$ . A discrepancy with numerical value (14) is explained by the fact that, near the depinning threshold, the soliton suffers appreciable deformation, while the analytical approach assumes the fixed shape (6).

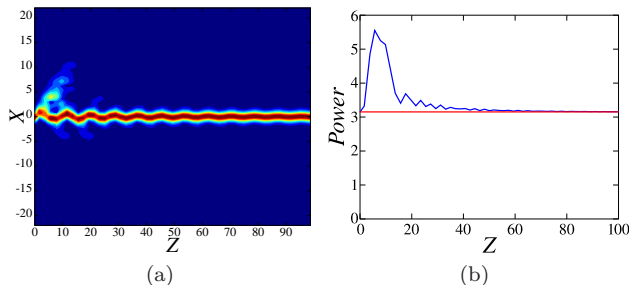


FIG. 2: (Color online) (a): The evolution of the local amplitude,  $|u(X, Z)|$ , in the cross section,  $Y = 0$ , of the fundamental soliton kicked with the under-threshold strength,  $k_0 = 1.61$  at  $\theta = 0$ . (b) The evolution of the total power in this case. The horizontal line show the powers for 1 quiescent fundamental soliton.

If the kick is sufficiently strong,  $k_0 > (k_0)_{\text{thr}}$ , the portion of the wave field passing the potential barrier has enough power to form a new dissipative soliton in the adjacent cell. The emerging secondary soliton may either stay in its cell, or keep moving through the lattice.

Figure 3 illustrates the creation of two new solitons at  $k_0 = 1.6878$ , which slightly exceeds the threshold value (14). This scenario can be summarized as follows:

- the initial soliton (or a part of it) passes the potential barrier and gets into the adjacent (second) cell;
- it then stays for some time in that cell;
- if the initial kick is not strong enough, the secondary soliton permanently stays at this location;
- if the kick is harder, the soliton again passes the potential barrier, getting into the third cell;
- a portion of the wave field of the secondary soliton stays in the second cell and grows into a full soliton in this cell;

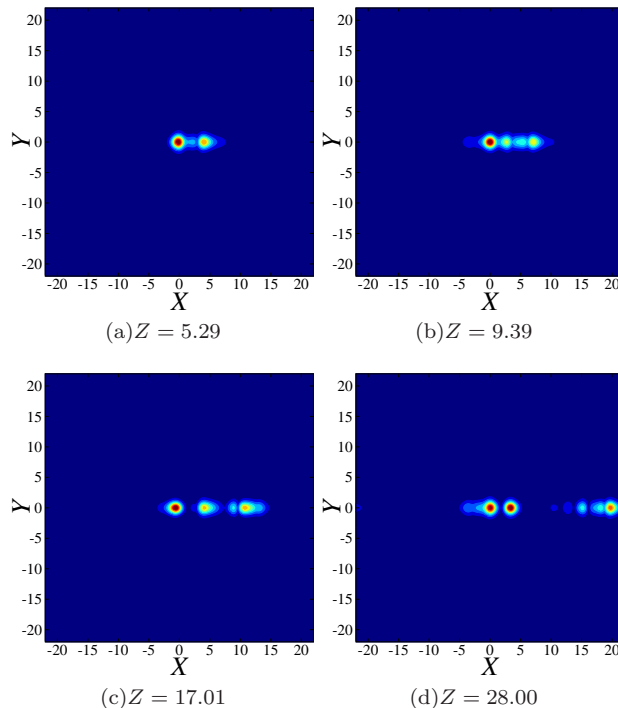


FIG. 3: (Color online) Evolution of the local field amplitude of the kicked soliton,  $|u(X, Y)|$ , for  $k_0 = 1.6878$  and  $\theta = 0$ . The field distributions are displayed at different values of propagation distance  $Z$ .

- if the kick is not sufficient to continue the filling of farther cells, oscillations of all the persistent solitons relax.

The present case is further illustrated in Fig. 4 by the plot for the evolution of the total power, which shows that  $P$  attains the first maximum at  $z = 31.78$ , and then oscillates. Every minimum correspond to the collision between the two solitons. For the sake of comparison, four horizontal lines in the figure mark the powers corresponding to the

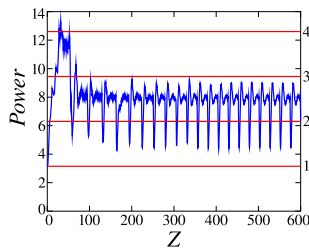


FIG. 4: (Color online) The evolution of the total power of the pattern in the case displayed in Fig. 3, with  $k_0 = 1.6878$  and  $\theta = 0$ . The horizontal lines show the powers for 1, 2, 3 and 4 quiescent fundamental solitons.

single stable soliton ( $P_{\text{sol}} \approx 3.15$ ), multiplied, respectively, by 1, 2, 3, or 4.

It has been found that solitons can duplicate several times, thus forming extended patterns in the form of soliton arrays. The increase of the kick's magnitude leads to the decrease of the number of the solitons forming this pattern, as the soliton moves faster and does not spend enough time in each cell to create a new soliton trapped in it. In particular, Fig. 5 demonstrates that only one soliton is generated at  $k_0 = 1.6872$  (recall that Fig. 3 appertains to  $k_0 = 1.6878$ ). Further, at  $k_0 = 2.082$  the soliton performs unhindered motion up to hitting the boundary, without leaving any stable pattern in its wake (not shown here in detail).

On the other hand, the smaller kick can initiate the creation of an arrayed pattern. This outcome of the evolution is shown in Fig. 6, where the array of five solitons is created, starting with the soliton initially kicked by  $k_0 = 1.694$ .

The emerging array remains in an excited state, featuring localized density waves running across it, as shown by means of the cross-section picture in Fig. 7). It is worthy to note that the wave is actually reflected from the last pinned soliton. Such localized density perturbations propagating through a chain of pinned solitons is similar to the

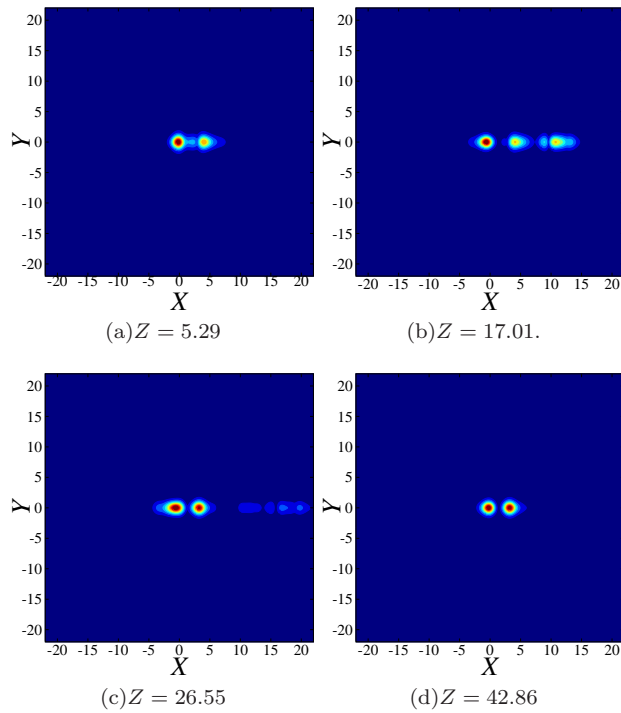


FIG. 5: (Color online) The same as in Fig. 3, but for  $k_0 = 1.6872$  and  $\theta = 0$ .

so-called “super-fluxons”, which were investigated experimentally and theoretically in arrays of fluxons (topological solitons, representing magnetic-flux quanta) pinned in a long Josephson junction with a periodic lattice of local defects [19].

### B. The dependence of the outcome of the evolution on the strength of the initial kick

Results of the systematic analysis of the model are summarized in Fig. 10, where the number of solitons in the stable arrayed patterns established by the end of the simulation, is plotted versus the initial kick  $k_0$  for  $\theta = 0$ . Additionally, intervals of the values of  $k_0$  corresponding to constant numbers of the solitons are given in Table I. In case the free soliton collides with the quiescent array, see the example in Figs. 8 and 9, the number of solitons was counted just before the first such collision. Otherwise, the number was recorded after any motion in the system would cease.

Number of solitons	Range of $k_0$
1	$k_0 \in [0, 1.6865]$
2	$k_0 \in [1.6867, 1.6875]$
3	$k_0 \in [1.6878, 1.6905]$
4	$k_0 \in [1.6907, 1.691]$
5	$k_0 \in [1.6911, 1.6925]$
6	$k_0 \in [1.6927, 1.6942]$
5	$k_0 \in [1.6945, 1.7201]$
4	$k_0 \in [1.7204, 1.7657]$
3	$k_0 \in [1.766, 1.866]$
2	$k_0 \in [1.867, 2.081]$
1	$k_0 \in [2.082, +\infty)$

TABLE I: The number of solitons in the final state versus  $k_0$ , for  $\theta = 0$ .

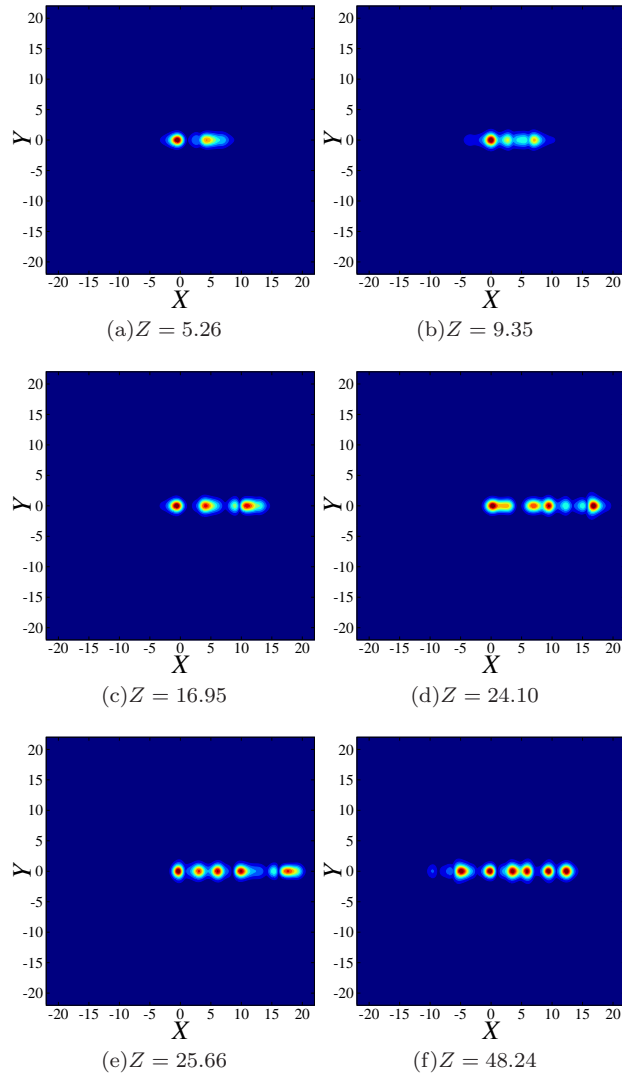


FIG. 6: (Color online) The same as in Figs. 3 and 5, but for  $k_0 = 1.694$ . In this case, the kicked soliton creates an arrayed pattern which extends.

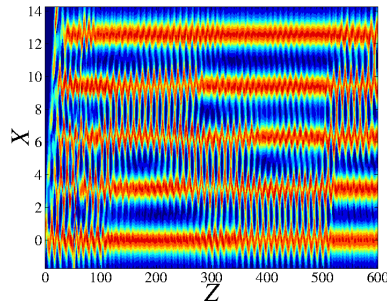


FIG. 7: (Color online) Evolution of the local amplitude,  $|u(X, Z)|$ , in the cross-section plane,  $Y = 0$ , at  $k_0 = 1.694$  and  $\theta = 0$ .

The results demonstrate that number of solitons in the established patterns rapidly increases from one at  $k_0 \leq (k_0)_{\text{thr}} \approx 1.6865$  [see Eq. (14)] to a maximum of five solitons, plus a sixth freely moving one, at  $k_0 = 1.6927$ . New solitons add to the established pattern according to the scenario outlined by the means of the bullet items in the previous subsection. Beyond this point, the number decreases by steps with an increasing length of the corresponding intervals

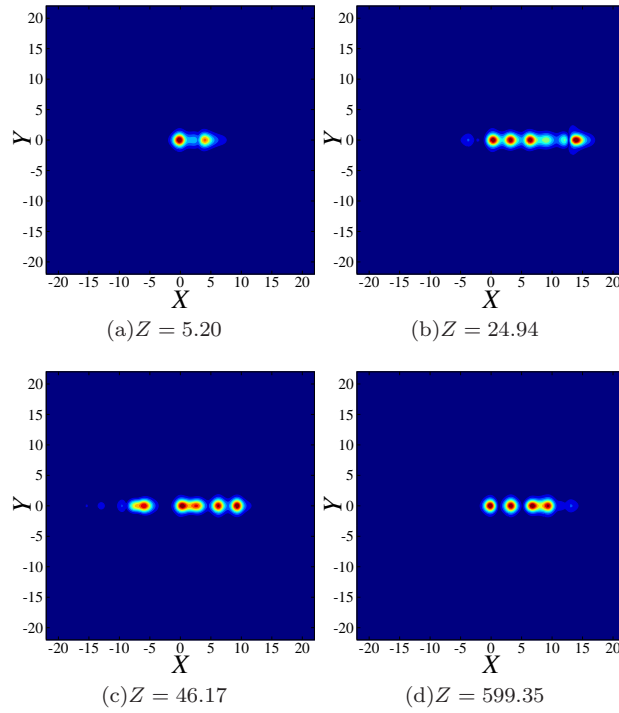


FIG. 8: (Color online) The same as in Fig. 6, but for  $k_0 = 1.705$ . In this case, a free soliton splits away from the quiescent array, then hits it from the other side, and gets absorbed by it.

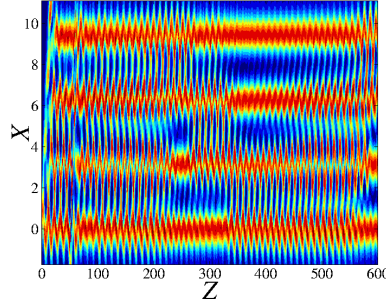


FIG. 9: (Color online) The top view of the same dynamical picture as in Fig. 8.

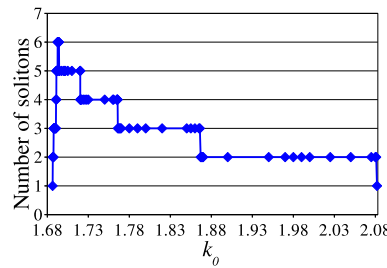


FIG. 10: (Color online) The graphical rendition of the same information which is presented in Table I: The number of solitons in the established pattern versus the kick's strength,  $k_0$ , at  $\theta = 0$ .

of the kick's strength, see Table I.

As mentioned above, the largest number of six solitons is reached at  $1.6927 < k_0 < 1.6942$  (see Figure 11(a)), with the averaged total power  $P = 23$ , see Fig. 11(b). The horizontal reference lines in this figure show the power levels



corresponding to a single quiescent soliton (recall  $P_{\text{sol}} \approx 3.15$ ), multiplied by factors from 1 to 7, which demonstrates that the total power of the six-soliton complex exceeds the seven-fold power of the single soliton. This is due to the fact that the energy of the moving soliton is roughly twice that of a soliton at rest.

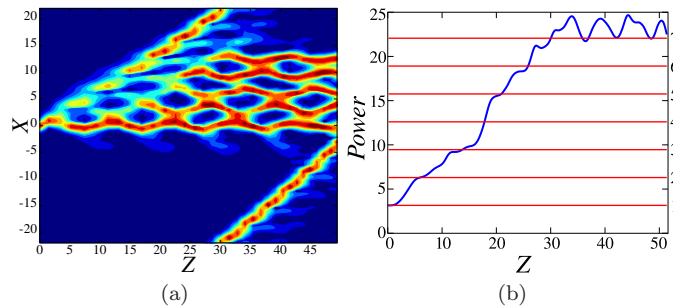


FIG. 11: (Color online) (a): The field amplitude,  $|u(X, Z)|$ , in the cross section  $Y = 0$ , and (b) the evolution of the total power, for the kick's strength  $k_0 = 1.693$  at  $\theta = 0$ , which leads to the establishment of the six-soliton pattern.

At  $k_0 \geq 2.082$ , the kicked soliton moves freely across the simulation domain, see Fig. 12(a). In this case, the figure demonstrates that the soliton's velocity increases, approaching a certain limit value. The computation of the velocity was performed by means of the Lagrange's interpolation of the numerical data to accurately identify the soliton's center. To display the results, small-scale oscillations of the velocity of the soliton passing the periodic potential (obviously, the velocity is largest and smallest when the solitons traverses the bottom and top points of the potential, respectively) have been smoothed down by averaging the dependence over about fifteen periods.

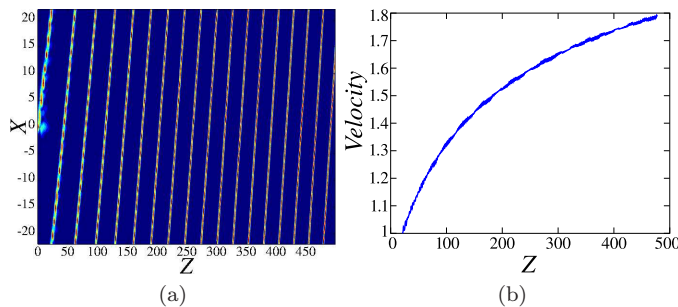


FIG. 12: (Color online) (a) The distribution of the field amplitude,  $|u(X, Z)|$  in cross section  $Y = 0$ , and (b) the evolution of the velocity of the fundamental soliton kicked by  $k_0 = 2.1$  at  $\theta = 0$ .

### C. The evolution initiated by an oblique kick

The application of the kick under an angle to the lattice, i.e., with  $\theta \neq 0$  [see Eq. (5)], was considered too. The results are summarized in Tables II and III for angles  $\theta = \pi/4$  (the kick oriented along the diagonal) and  $\theta = \pi/8$ , respectively.

Number of solitons	Range of $k_0$
1	$k_0 \in [0, 2.355]$
0	$k_0 \in [2.36, 4.337]$
1	$k_0 \in [4.563, 10]$

TABLE II: The same as in Table I, but for the diagonal kick, with  $\theta = \pi/4$ .

For  $\theta = \pi/4$ , the initial soliton remains pinned at  $k_0 \leq (k_0)_{\text{thr}} (\theta = \pi/4) = 2.166$ , and it is destroyed at  $2.25 < k_0 < 4.337$ . At  $k_0 > 4.337$ , the single soliton survives, moving freely along the diagonal direction. Thus, the final number of the solitons in this case is 1 or 0 (see Table II), and no new solitons are generated. As concerns the comparison with

the analytical prediction (13), it yields  $(k_0)_{\text{thr}}(\theta = \pi/4) \approx 1.87$ , which, as well as in the case of  $\theta = 0$ , is somewhat lower than its numerical counterpart.

The kicks with much larger values of  $k_0$  (one or two orders of magnitude higher than in Table II) cause the generation of dark-soliton structures, supported by a nonzero background filling the entire domain (the total power may then exceed that of the single soliton by a factor  $\sim 1000$ ). Inspection of Fig. 13(a) reveals stable holes in the continuous background, whose centers coincide with phase singularities (see Fig. 13(b)). These holes represent the 2D dark solitons (to say more accurately, dark-soliton vortices).

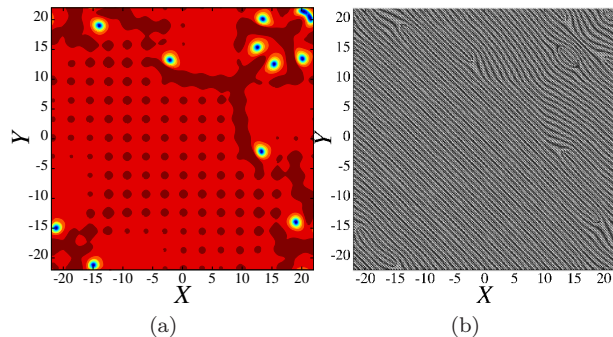


FIG. 13: (Color online) The distribution of the field amplitude,  $|u(X, Y)|$  (a) and phase (b) in the pattern produced by kicking the fundamental soliton in the diagonal direction ( $\theta = \pi/4$ ) very hard, with  $k_0 = 100$ . The picture corresponds to evolution distance  $Z = 199.90$ .

Number of solitons			Range of $k_0$
Total	Along X	Along Y	
1	0	0	$k_0 \in [0, 1.816]$
3	2	0	$k_0 = 1.974$
2	1	0	$k_0 = 2.1$
1	0	0	$k_0 \in [2.224, 4.569]$
0	0	0	$k_0 \in [4.816, 5.804]$
1	0	0	$k_0 \in [6.05, \infty)$

TABLE III: The same as in Table II, but for the oblique kick oriented under angle  $\theta = \pi/8$ .

One can see in Table III the numbers of new solitons created along  $X$  or  $Y$  direction. The total count have a soliton more, it corresponds to the original one. Further, for the kick applied at angle  $\theta = \pi/8$ , the simulations demonstrate that the soliton remains pinned at  $k_0 \leq (k_0)_{\text{thr}}(\theta = \pi/8) = 1.816$ , while the analytical approximation (13) for the same case predicts  $(k_0)_{\text{thr}}(\theta = \pi/8) \approx 1.54$ . Above the threshold, the creation of new solitons occurs, similar to the case of  $\theta = 0$ , in contrast with  $\theta = \pi/4$ . The largest three-soliton pattern is created at  $k_0 = 1.974$ , which is composed of two oscillating non-propagating solitons and a freely moving one, as shown in Fig. 14. At  $k_0 = 2.1$ , the dynamics again amounts to the motion of a single soliton. We stress that, despite the oblique direction of the kick in this case, all the solitons move strictly along the  $X$ -axis, see Fig. 14. A harder kick,

$$4.816 < k_0 < 5.804, \quad (15)$$

destroys the soliton (its power at first increases, as it moves across the first PN barrier, and then decays to zero).

At still higher  $k_0$ , the soliton survives the kick, but in this case its trajectory is curvilinear in the plane of  $(X, Y)$ . The latter property is illustrated in Fig. 15 by the evolution of the trajectory of the soliton's center. For the sake of comparison, we add the rectilinear trajectory corresponding of an angle  $\theta = \pi/8$ .

It is relevant to compare the number of solitons in the patterns generated by the simulations for  $\theta = 0$  and  $\theta = \pi/8$ . For both cases, these numbers are presented, as functions of projection  $k_{0x} \equiv k_0 \cos(\theta)$  of the kick vector onto the  $X$ -axis, in Table IV. It is seen that the dependences of the soliton number on  $k_{0x}$  are quite similar for  $\theta = 0$  and  $\theta = \pi/8$ . A difference appears when the soliton is destroyed with  $\theta = \pi/8$  and it is conserve with  $\theta = 0$ .

Further, the evolution of the soliton's velocity for different strengths of the kick is shown in Fig. 16. Recall that, for  $\theta = \pi/8$ , there are two domains of values of  $k_0$  in which the soliton moves, separated by interval (15) in which it

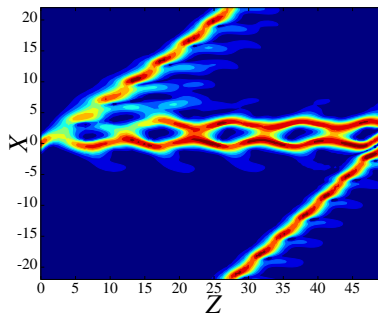


FIG. 14: (Color online) The local field amplitude,  $|u(X, Z)|$ , in the cross section  $Y = 0$ , for  $k_0 = 1.9743$  and  $\theta = \pi/8$ .

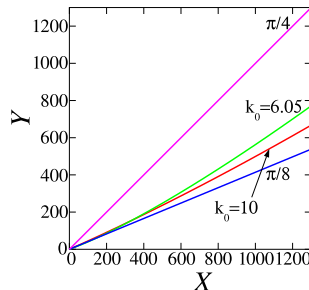


FIG. 15: (Color online) Trajectory of every solitons and two fictional trajectories with  $\theta = \pi/8$  and  $\theta = \pi/4$ .

Range of the norm $k_0$	Range of the projection $k_{0x}$	Number of solitons for $\theta = 0$	Number of solitons for $\theta = \pi/8$
[0, 1.816]	[0, 1.6778]	1	1
1.974	1.8237	3	3
2.1	1.9401	2	2
[2.224, 4.569]	[2.0547, 4.2212]	1	1
[4.816, 5.804]	[4.4494, 5.3622]	1	0

TABLE IV: The number of solitons versus the  $k_{0x}$  component of the kick vector, for two different orientations,  $\theta = 0$  and  $\pi/8$ .

is destroyed by the kick. It is observed that the solitons accelerate and decelerate below and above the nonexistence interval (15), respectively, but eventually the velocity approaches a constant value. Moreover, the picture suggests that, as a result of the long evolution, the velocity is pulled to either of the two discrete values,  $\approx 2$  or  $\approx 3$ . As said above, these velocities (in other words, the values of  $k_0$  which can directly produce such velocities, see straight horizontal lines in Fig. 16) correspond to the single soliton moving along the  $X$  axis, rather than under an angle to it. The conclusion that the system relaxes to discrete values of the velocity is natural, as the dissipative system should give rise to a single or several isolated *attractors*, rather than a continuous family of states with an arbitrary velocity.

A similar behavior is observed for other orientations of the kick,  $\theta = \pi/4$  and  $\theta = 0$ , see the curves labeled by these values of  $\theta$  in Fig. 16, and also Fig. 12(b). Again, the velocity asymptotically approaches the same discrete values, close to 2 and 3, with the acceleration or deceleration below and above these values, respectively. For solitons with  $\theta = \pi/4$ , in the established regime, they move along the diagonal keeping the value of  $\theta$ .

#### IV. COLLISIONS BETWEEN MOVING SOLITONS AND STANDING PATTERNS

One of generic dynamical patterns identified above features a standing multi-soliton structure and a freely moving soliton, see Fig. 14. In the case of periodic boundary conditions, the free soliton will hit the standing structure from the opposite side. Two generic scenarios of the interactions have been identified in this case, namely, an elastic collision, with the incident soliton keeping the original velocity and direction after the interaction, and absorption of

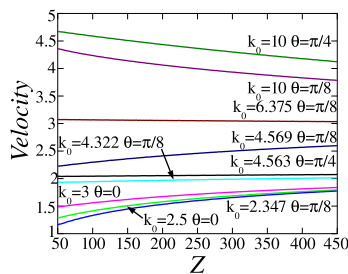


FIG. 16: (Color online) The soliton's velocity as a function of  $Z$  at various values of  $k_0$  and  $\theta$ .

the incident soliton by the standing pattern, see Figs. 17(a) and 17(b), respectively. More complex collision scenarios

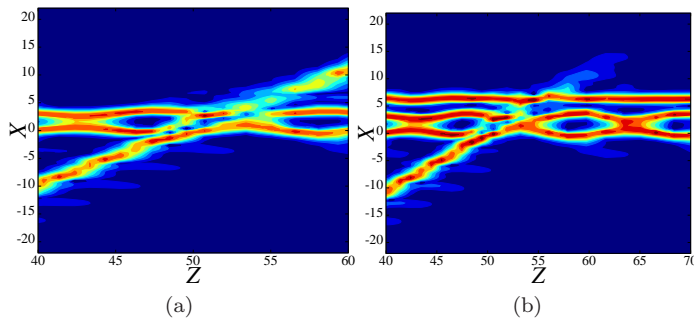


FIG. 17: (Color online) Basic types of interactions between a moving soliton and a standing multi-soliton structure: (a) An elastic collision, at  $k_0 = 1.8$  and  $\theta = 0$ ; (b) the absorption of the incident soliton, at  $k_0 = 1.765$  and  $\theta = 0$ .

were observed too, with several elastic or quasi-elastic collisions that end up with the eventual absorption of the free soliton. Outcomes of the collisions are summarized in Table V (the range of  $k_0 > 2.081$  is not shown in the table, as only the single soliton exists in this case). At  $1.766 < k_0 < 1.86$ , several elastic collisions, from 1 to 5, the number of which alternates in an apparently random fashion, are observed before the absorption is registered. This scenario is labeled “Newton’s cradle with damping” in Table V. At  $k_0 > 1.86$ , the collision is elastic and persists to occur periodically, as in the ordinary Newton’s cradle, see Fig. 18. A special case is the one corresponding to the creation

Collision type	Range of $k_0$
absorption	$k_0 = 1.6879$
Newton’s cradle with damping	$k_0 = 1.6909$
absorption	$k_0 = 1.692$
complex	$k_0 = 1.693$
absorption	$k_0 \in [1.695, 1.765]$
Newton’s cradle with damping	$k_0 \in [1.766, 1.86]$
Newton’s cradle	$k_0 \in [1.866, 2.081]$

TABLE V: Collision types versus the magnitude of the initial kick,  $k_0$ .

of the largest number of solitons at  $k_0 = 1.693$ , as shown above. The collision pattern is quite complex in this case, as shown in Fig. 19(a). Both elastic collisions (at  $z \simeq 100$  and  $200$ ) and absorptions (at  $z \simeq 475$ ) are observed. An unexpected feature of the process is the reversal of the direction of motion of two solitons around  $z \simeq 300$ . The whole patterns eventually relaxes into an array built of six solitons, which is confirmed by the power-evolution plot in Fig. 19(b). In the case of elastic collisions between two solitons recurring indefinitely long, we have checked if the velocity of the transmitted soliton is the same as that of the incident one. To this end, it is relevant to consider the case of  $k_0 = 1.974$  and  $\theta = 0$ , for which the scenario is almost identical to that shown in Fig. 18. It is seen in Fig. 20(a) that each collision leads to the exchange of velocities between the two solitons, as for colliding hard particles. In addition, we identified the velocity of the center of mass of the two-solitons set. Figure 20(b) shows that the latter velocity gradually increases within the sequence of collisions. Accordingly, the solitons’ velocities approach one of

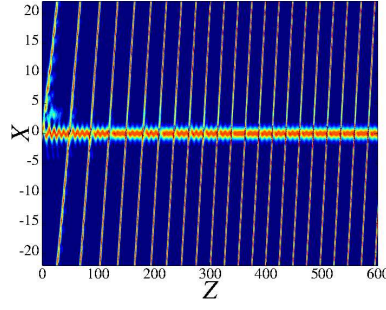


FIG. 18: (Color online) An example of periodic elastic collisions corresponding to the Newton's cradle, at  $k_0 = 1.867$  and  $\theta = 0$ .

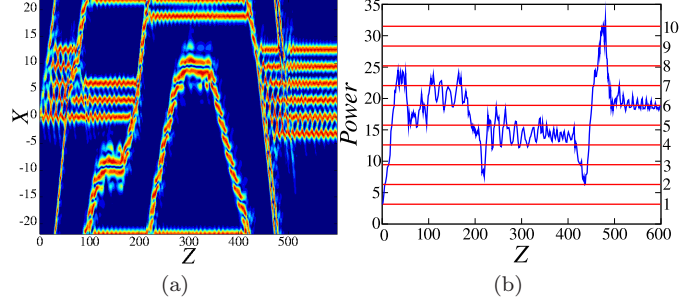


FIG. 19: (Color online) (a): The distribution of the field,  $|u(X, Z)|$ , in the cross section  $Y = 0$ ; (b): the total power versus  $Z$  of a fundamental soliton with  $k_0 = 1.693$  and  $\theta = 0$ . In panel (b), horizontal lines show the multiple powers of the quiescent fundamental soliton.

the above-mentioned discrete values characteristic to the established motion of single solitons. It stabilizes at a value close to 1.

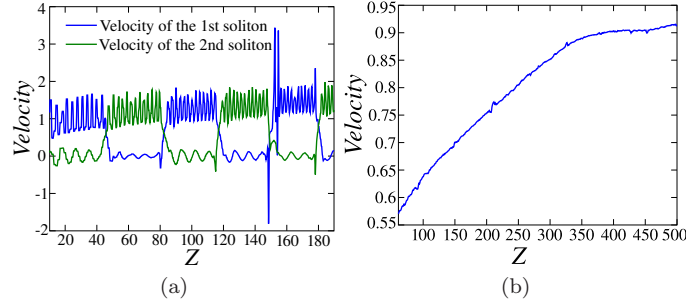


FIG. 20: (Color online) Velocities of each soliton (a) and center of mass (b) versus  $Z$  for the pair of periodically colliding fundamental solitons. Here  $k_0 = 1.974$  and  $\theta = 0$ .

## V. CONCLUSIONS

The subject of this work is the mobility of 2D dissipative solitons in the CGL (complex Ginzburg-Landau) equation which includes the spatially periodic potential. This equation models the bulk lasing medium with a built-in transverse grating. The soliton was set in motion by the application of the kick, which corresponds to a tilt of the seed beam. The mobility implies the possibility to generate stable oblique beams in the medium. Further, the advancement of the kicked soliton may be used to create various arrayed patterns in the wake of the soliton hopping between the potential cells. The depinning threshold, i.e., the smallest strength of the kick which sets the quiescent soliton into motion, was found by means of simulations, and also with the help of the analytical approximation, based on the estimate of the condition for the passage of the kicked object across the PN (Peierls-Nabarro) potential. The

dependence of the threshold on the orientation of the kick with respect to the underlying lattice potential was studied too. Various pattern-formation scenarios have been identified above the threshold, with the number of solitons in stationary arrayed patterns varying from one to six. Freely moving solitons may eventually assume two distinct values of the velocity, which represent coexisting attractors in this dissipative system. Also studied were elastic and inelastic collisions between the free soliton and stationary multi-soliton structures. A natural extension of the present work will deal with the dynamics initiated by the application of the kick to stable vortices pinned to the sites of the lattice potential.

### Acknowledgments

This work was supported, in a part, by grant No. 3-6738 from High Council for scientific and technological cooperation between France and Israel. The work of DM was supported in part by a Senior Chair Grant from the Région Pays de Loire, France. Support from the Romanian Ministry of Education and Research (Project PN-II-ID-PCE-2011-3-0083) is also acknowledged.

- 
- [1] N. N. Rosanov, *Spatial Hysteresis and Optical Patterns* (Springer, Berlin, 2002); S. Barland *et al.*, *Nature* (London) **419**, 699 (2002); Z. Bakonyi, D. Michaelis, U. Peschel, G. Onishchukov, and F. Lederer, *J. Opt. Soc. Am. B* **19**, 487 (2002); E. A. Ultanir, G. I. Stegeman, D. Michaelis, C. H. Lange, and F. Lederer, *Phys. Rev. Lett.* **90**, 253903 (2003); P. Mandel and M. Tlidi, *J. Opt. B: Quantum Semiclass. Opt.* **6**, R60 (2004); N. N. Rosanov, S. V. Fedorov, and A. N. Shatsev, *Appl. Phys. B* **81**, 937 (2005); C. O. Weiss and Ye. Larionova, *Rep. Progr. Phys.* **70**, 255 (2007); N. Veretenov and M. Tlidi, *Phys. Rev. A* **80**, 023822 (2009); P. Genevet, S. Barland, M. Giudici, and J. R. Tredicce, *Phys. Rev. Lett.* **104**, 223902 (2010).
- [2] N. Lazarides and G. P. Tsironis, *Phys. Rev. E* **71**, 036614 (2005); Y. M. Liu, G. Bartal, D. A. Genov, and X. Zhang, *Phys. Rev. Lett.* **99**, 153901 (2007); E. Feigenbaum and M. Orenstein, *Opt. Lett.* **32**, 674 (2007); I. R. Gabitov, A. O. Korotkevich, A. I. Maimistov, and J. B. McMahon, *Appl. Phys. A* **89**, 277 (2007); A. R. Davoyan, I. V. Shadrivov, and Y. S. Kivshar, *Opt. Exp.* **17**, 21732 (2009); K. Y. Bliokh, Y. P. Bliokh, and A. Ferrando, *Phys. Rev. A* **79**, 041803 (2009); E. V. Kazantseva and A. I. Maimistov, *ibid.* **79**, 033812 (2009); Y.-Y. Lin, R.-K. Lee, and Y. S. Kivshar, *Opt. Lett.* **34**, 2982 (2009); A. Marini and D. V. Skryabin, *ibid.* **81**, 033850 (2010); A. Marini, D. V. Skryabin, and B. A. Malomed, *Opt. Exp.* **19**, 6616 (2011).
- [3] N. Akhmediev and A. Ankiewicz (Eds.), *Dissipative Solitons*, *Lect. Notes Phys.* **661**, Springer, Berlin, 2005; N. Akhmediev and A. Ankiewicz (Eds.), *Dissipative Solitons: From Optics to Biology and Medicine*, *Lect. Notes Phys.* **751**, Springer, Berlin, 2008.
- [4] J. Anglin, *Phys. Rev. Lett.* **79**, 6 (1997); F. T. Arecchi, J. Bragard, and L. M. Castellano, *Opt. Commun.* **179**, 149 (2000); J. Keeling and N. G. Berloff, *Phys. Rev. Lett.* **100**, 250401 (2008); B. A. Malomed, O. Dzyapko, V. E. Demidov, and S. O. Demokritov, *Phys. Rev. B* **81**, 024418 (2010); H. Deng, H. Haug, and Y. Yamamoto, *Rev. Mod. Phys.* **82**, 1489 (2010); B. Deveaud-Plédran, *J. Opt. Soc. Am. B* **29**, A138 (2012).
- [5] I. S. Aranson and L. Kramer, *Rev. Mod. Phys.* **74**, 99 (2002); B. A. Malomed, in *Encyclopedia of Nonlinear Science*, p. 157. A. Scott (Ed.), Routledge, New York, 2005.
- [6] V. I. Petviashvili and A. M. Sergeev, *Dokl. AN SSSR* **276**, 1380 (1984) [*Sov. Phys. Doklady* **29**, 493 (1984)].
- [7] O. Thual and S. Fauve, *J. Phys. (Paris)* **49**, 1829 (1988); S. Fauve and O. Thual, *Phys. Rev. Lett.* **64**, 282 (1990); W. van Saarloos and P. C. Hohenberg, *Phys. Rev. Lett.* **64**, 749 (1990); V. Hakim, P. Jakobsen, and Y. Pomeau, *Europhys. Lett.* **11**, 19 (1990); B. A. Malomed and A. A. Nepomnyashchy, *Phys. Rev. A* **42**, 6009 (1990); P. Marcq, H. Chaté, R. Conte, *Physica D* **73**, 305 (1994); N. Akhmediev and V. V. Afanasjev, *Phys. Rev. Lett.* **75**, 2320 (1995); H. R. Brand and R. J. Deissler, *Phys. Rev. Lett.* **63**, 2801 (1989); V. V. Afanasjev, N. Akhmediev, and J. M. Soto-Crespo, *Phys. Rev. E* **53**, 1931 (1996); J. M. Soto-Crespo, N. Akhmediev, and A. Ankiewicz, *Phys. Rev. Lett.* **85**, 2937 (2000); H. Leblond, A. Komarov, M. Salhi, A. Haboucha, and F. Sanchez, *J. Opt. A: Pure Appl. Opt.* **8**, 319 (2006); W. H. Renninger, A. Chong, and F. W. Wise, *Phys. Rev. A* **77**, 023814 (2008); J. M. Soto-Crespo, N. Akhmediev, C. Mejia-Cortes, and N. Devine, *Opt. Express* **17**, 4236 (2009); D. Mihalache, *Proc. Romanian Acad. A* **11**, 142 (2010); Y. J. He, B. A. Malomed, D. Mihalache, F. W. Ye, and B. B. Hu, *J. Opt. Soc. Am. B* **27**, 1266 (2010); D. Mihalache, *Rom. Rep. Phys.* **63**, 325 (2011); C. Mejia-Cortes, J. M. Soto-Crespo, R. A. Vicencio, and M. I. Molina, *Phys. Rev. A* **83**, 043837 (2011); D. Mihalache, *Rom. J. Phys.* **57**, 352 (2012). O. V. Borovkova, V. E. Lobanov, Y. V. Kartashov, and L. Torner, *Phys. Rev. A* **85**, 023814 (2012).
- [8] L.-C. Crasovan, B. A. Malomed, and D. Mihalache, *Phys. Rev. E* **63**, 016605 (2001); *Phys. Lett. A* **289**, 59 (2001); D. Mihalache, D. Mazilu, F. Lederer, Y. V. Kartashov, L.-C. Crasovan, L. Torner, and B. A. Malomed, *Phys. Rev. Lett.* **97**, 073904 (2006); D. Mihalache, D. Mazilu, F. Lederer, H. Leblond, and B. A. Malomed, *Phys. Rev. A* **76**, 045803 (2007); *ibid.* **75**, 033811 (2007); D. Mihalache and D. Mazilu, *Rom. Rep. Phys.* **60**, 749 (2008).
- [9] V. Skarka and N. B. Aleksić, *Phys. Rev. Lett.* **96**, 013903 (2006); N. B. Aleksić, V. Skarka, D. V. Timotijević, and D. Gauthier, *Phys. Rev. A* **75**, 061802 (2007); V. Skarka, D. V. Timotijević, and N. B. Aleksić, *J. Opt. A: Pure Appl. Opt.*

- 10**, 075102 (2008); V. Skarka, N. B. Aleksić, H. Leblond, B. A. Malomed, and D. Mihalache, Phys. Rev. Lett. **105**, 213901 (2010).
- [10] H. Leblond, B. A. Malomed, and D. Mihalache, Phys. Rev. A **80**, 033835 (2009).
- [11] A. Szameit, J. Burghoff, T. Pertsch, S. Nolte, and A. Tünnermann, Opt. Exp. **14**, 6055 (2006).
- [12] J. W. Fleischer, M. Segev, N. K. Efremidis, and D. N. Christodoulides, Nature **422**, 147 (2003).
- [13] D. Mihalache, D. Mazilu, V. Skarka, B. A. Malomed, H. Leblond, N. B. Aleksić, and F. Lederer, Phys. Rev. A **82**, 023813 (2010).
- [14] D. Mihalache, D. Mazilu, F. Lederer, H. Leblond, and B. A. Malomed, Phys. Rev. A **81**, 025801 (2010).
- [15] L. Bergé, Phys. Rep. **303**, 260 (1998).
- [16] M. Desaix, D. Anderson, and M. Lisak, J. Opt. Soc. Am. B **8**, 2082 (1991).
- [17] B. A. Malomed, Physica D **29**, 155 (1987).
- [18] H. Sakaguchi, Physica D **210**, 138 (2005).
- [19] A. V. Ustinov, Phys. Lett. A **136**, 155 (1989); B. A. Malomed, Phys. Rev. B **41**, 26166 (1990); A. Shnirman, Z. Hermon, A. V. Ustinov, B. A. Malomed, and E. Ben-Jacob, *ibid.* B **50**, 12793 (1994).